Smart flapping wing using Macro-Fiber Composite actuators

Dae-Kwan Kim, and Jae-Hung Han

Department of Aerospace Engineering, Korea Advanced Institute of Science and Technology
Daejeon 305-701, Republic of Korea

< Article Info. >

Publication Title	**SPIE 13th Annual Symposium Smart Structures and Materials**
Journal Homepage	http://spie.org/
Publication Year	**2006**
Volume/Issue	
Paginations	
DOI	http://dx.doi.org/10.1117/12.658117
Further Info.	http://sss.kaist.ac.kr/
Remark	**This PDF file is based on the final submission to the publisher, and there might be slight change from the final form provided by the publisher.**

PROCEEDINGS OF SPIE on CD-ROM

Smart Structures and Materials 2006

26 February–2 March 2006
San Diego, California USA

Vols. 6166–6174

- Getting Started
- Conferences
- Search
- Copyright

Volume 6173: Smart Structures and Materials 2006: Smart Structures and Integrated Systems

Chair/Editor: Yuji Matsuzaki

Smart flapping wing using Macro-Fiber Composite actuators

Dae-Kwan Kim*, and Jae-Hung Han†

Department of Aerospace Engineering, Korea Advanced Institute of Science and Technology
Daejeon 305-701, Republic of Korea

ABSTRACT

In the present study, we have developed a smart flapping wing with a MFC (macro-fiber composites) actuator. To mimic the flying mechanisms of nature's flyers such as birds or insects, the aerodynamic characteristics related to the birds and ornithopters are investigated. To measure the aerodynamic forces of flapping devices, a test stand consisting of two loadcells is manufactured, and the dynamic tests are performed for an onithopter. The smart flapping wing is designed and manufactured using composite materials and MFC actuators. The camber of the wing can be changed by using the surface actuators to enhance the aerodynamic performance of the wing. Finally, aerodynamic tests are performed in a subsonic wind tunnel to evaluate the dynamic characteristics of the smart flapping wing. Experimental results show that unsteady flow effects are increased with low velocity in high flapping frequency regions, and that the deformation of the wing surface generated by the MFC is enough to control the lift and thrust. The lift generated by the smart flapping wing can be increased by 20% when the MFC is actuated.

Keywords: Bird flight, flapping wing, Macro Fiber Composite, biomimetic design

1. INTRODUCTION

Bird and insect flight has fascinated humans for many centuries, and the imitation of their flapping wing flight has been the oldest aeronautical dream. The biological flapping flight, which has evolved over 150 million years, is one of the nature's optimized locomotion experiments. Because of the aerodynamic and mechanical complexity, however, complete and exact analysis of the flapping flight is not available [1].

One of the methods to make a successful flapping vehicle is to evaluate and mimic the nature's flyers such as insects, birds or bats. Much effort has been made for flapping flight vehicles named ornithopter by using the biomimetic designs. Pornsin-sirirak et al. [2,3] developed a palm-sized onithopter named "Microbat". Its wings were manufactured by using MEMS technology, and the aerodynamic forces of the wings were measured by static and dynamic tests. SMA (Shape-memory-alloy) wires were used as muscle wires to control the elevator and rudder of the battery-powered ornithopter with a radio control system. The total weight was 12.5g and the flight duration of 49 seconds was achieved. Liger et al. [4,5] manufactured passive and adaptive valves by using MEMS technology. The wing skins were integrated with the electrostatic check-valves to control the distribution of the pressure on the wings during flapping. Jones et al. [6-8] developed a micro air vehicle which was propelled by a pair of flapping wings. The wings flapped in counterphase, and generated ground effect and stall suppression effect which increased the flight efficiency. Park et al. [9,10] manufactured flapping devices actuated by IPMC (Ionic Polymer Metal Composite) and LIPCA (Lighweight Piezo-Composite Actuator) of which actuation displacements were amplified by a linkage system. Flapping tests were performed to investigate the performance of the devices.

Most of the ornithopters have flexible wings and use the flapping motion which is one of the main wing motions of birds or insects. Unlike the nature's flyers, however, when their flapping axes are horizontal, the wings generate very little mean lift which is not enough to sustain their weight.

In this paper, the differences of the flapping flight between birds and ornithopters are described. To mimic the flapping motion of the birds, a smart flapping wing is designed and manufactured by using the graphite/epoxy composite

* Graduate Research Assistant, dkk@asdl.kaist.ac.kr.

† Assistant Professor, jaehunghan@kaist.ac.kr; 82 42 869-3723; fax 82 42 869-3710; Department of Aerospace Engineering, Korea Advanced Institute of Science and Technology, 373-1 Guseong-dong, Yuseong-gu, Daejeon, 305-701, Korea.

Smart Structures and Materials 2006: Smart Structures and Integrated Systems,
edited by Yuji Matsuzaki, Proc. of SPIE Vol. 6173, 61730F, (2006) · 0277-786X/06/$15
doi: 10.1117/12.658117

material and a MFC actuator. A dynamic test stand is manufactured to measure the aerodynamic forces of flapping devices, and wind tunnel tests for the wing are performed to investigate the aerodynamic characteristics and the performance of the surface actuators.

2. UNSTEADY AERODYNAMICS

2.1 Bird flight

Conventional airplanes with fixed wings use simple forward motion relative to the air to generate the lift. Traditional aerodynamic analysis can be used to predict the surface forces on the wings. However, flapping flight is quite complicated so that a complete and exact analysis for the flight is not available. In biological flight, the wings not only move forward relative to the air but also flap up and down, plunge, and sweep [1]. The birds, nature's optimized flying machines, have the wings of which cross sections are similar to the fixed wing airfoil, but insects have almost flat and flexible wings with corrugation which increases the natural frequency of the torsional deformation [11]. In the bird flight, a bound wing vortex and translational circulation are assumed to generate aerodynamic forces unlike insects [12]. There are three important motions in addition to the bird's forward motion: flapping, twisting and folding motions. They use these motions to produce large lift, thrust and effective incident angle, and to reduce drag throughout the wing stroke. By adaptation of skeletal and muscular systems as shown in Figure 1, they can also generate additional flight motions such as modification and reversal of camber between upward and downward strokes, wing area expansion and contraction, and transverse bending.

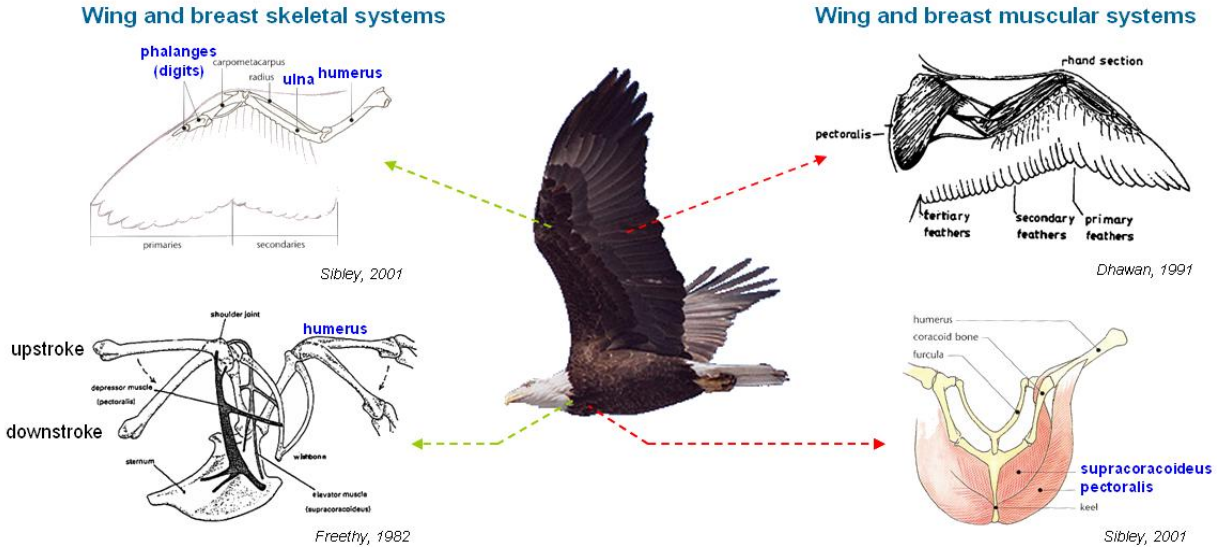

Figure 1: Bird's skeletal and muscular systems.

2.2 Ornithopter flight

In ornithopter flight, the flapping and twisting motions are mainly used to produce aerodynamic forces. If the artificial flapping machine has a flexible wing, the twisting motion can be generated automatically throughout the flapping motion. The wing generates positive horizontal forces relative to the flapping axis during the entire wing-stroke, but the vertical forces are produced in reciprocally opposite directions during up and down strokes. When the flapping axes are horizontal, therefore, the wing generates very little lift, even if cambered ribs are incorporated in the structure unlike birds as shown in Table 1 [13]. Therefore, most ornithopters are operated with the flapping axis vectored by adjusting the mass center or the stabilizer to achieve a positive trim angle as shown in Figure 2. The lifted flapping axis generates a vertical component force of the average resultant force, which is utilized as some of lift. It also makes effective angle of attack of the wing, so additional lift can be produced to sustain the flight.

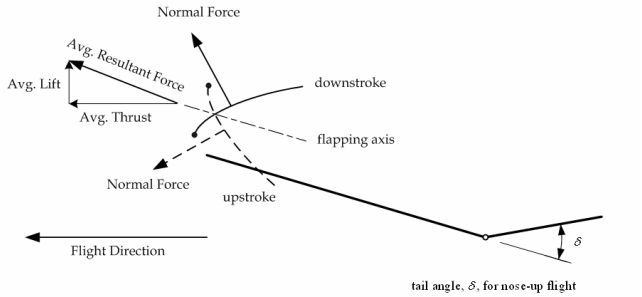

Figure 2: Force diagram for Penaud-type ornithopter. Modified from DeLaurier [13].

Table 1: Comparison of aerodynamic forces between ornithopters and birds at horizontal flapping axis.

Stroke	Ornithopters		Birds	
	Lift	Thrust	Lift	Thrust
Down	++	++	++	++
Up	−−	++	+	−
Sum		++++	+++	+

However, cruising birds and bats fly with horizontal flapping axis and their flight efficiency is fairly higher than that of the ornithopters. It is one of the objectives of this research to produce the positive mean lift with horizontal flapping axis like birds by using the biomimetic design.

3. AERODYNAMIC FORCES OF ORNITHOPTER

3.1 Test stand

The test stand is designed and manufactured to measure the vertical and horizontal aerodynamic forces, lift and thrust, of flapping devices. It consists of two loadcells that are combined together in perpendicular direction as shown in figure 3. The loadcell rated capacity is 6kg and non-linearity is less than 0.02%. Flapping devices are fixed at the test mount which can be used to adjust the angle of attack from -10^o to 20^o. Using the test stand, the lift and thrust can be measured simultaneously during flapping motion.

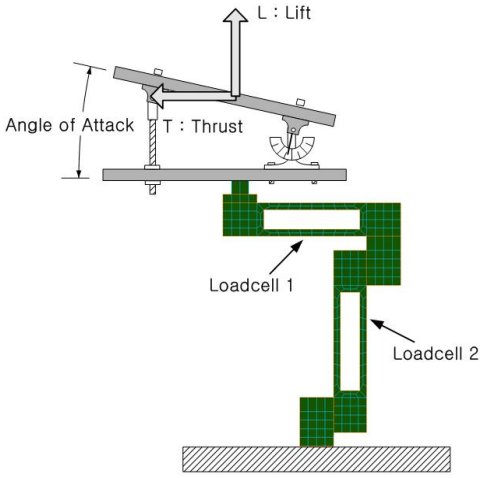

Figure 3: Configuration of test stand.

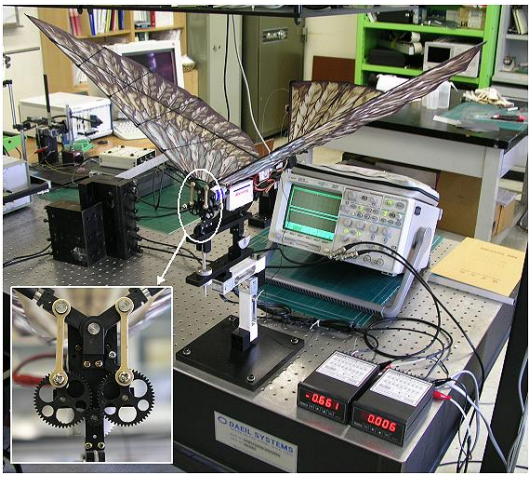

Figure 4: Experimental setup of flapping motion test. The insect is the transmission system of Cybird.

3.2 Onithopter test

For the first flapping test, a commercial ornithopter named Cybird-P2, made by Neuros Co. Ltd. in Korea, is used. It is a Li-Poly battery powered ornithopter with a 3Ch radio control system. The span of the wing is 990 mm, the total weight is 290 g and maximum flight duration is 18 minutes. The flapping motion is generated by a transmission system shown in Figure 4 insert, which converts the rotary motion of the driving DC motor into the flapping motion. The flapping

frequency can be controlled by varying the drive signal to the motor. The flapping angle is measured by the use of a laser Doppler vibrometer (OFV-3001/303), and all signals are acquired by the use of DSP board (dSPACE DS1103).

The flapping test is performed at zero angle of attack and zero velocity conditions. The flapping frequency is varied from 2 to 8.4 Hz. Figure 5 shows the time histories of lift, thrust and flapping angle measured from the flapping test. From the result, it is clear that the lift has almost the same frequency as the flapping motion and the thrust frequency is two times of flapping frequency. There are flat lift regions during the down-ward motion of the wing, which may be generated by the ground effect. The phase shift between lift and flapping angle for the variation of flapping frequency can not be exactly explained, because there are so many parameters affecting them such as flexible and 3D wing effect, ground effect, vortex attachment, asymmetric motion, and so on. Figure 6 shows the mean lift and thrust values for the variation of the flapping angle. The thrust values are proportional to the flapping frequency, but the lift mean value is almost zero. This result clearly demonstrates that when the flapping axis is horizontal, the wing generates positive thrust and very little lift which is not enough to sustain the flight as explained earlier.

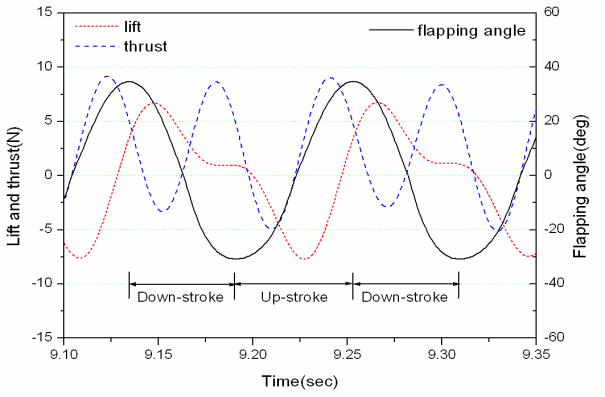

Figure 5: Comparison of lift, thrust and flapping angle at 8.4 Hz.

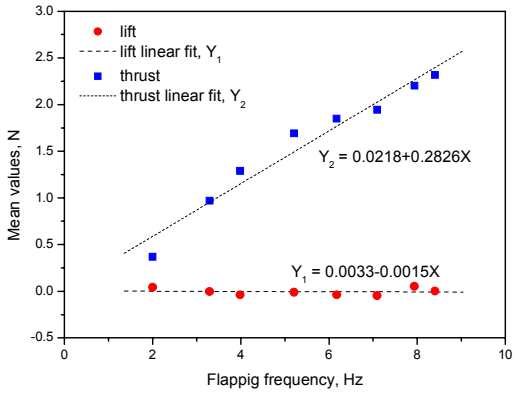

Figure 6: Flapping frequency vs. mean lift and thrust values.

4. SMART FLAPPING WING

4.1 Smart wing design

A smart flapping wing with MFC actuators is manufactured as shown in figure 7. The wing is designed from the structural analysis of the wing model based on the analogy between thermal strains and piezoelectric strains under MSC/NASTRAN [14]. The wing semi-span is 27 cm and the aspect ratio is 4.3. The wing consists of graphite/epoxy composite frames and flexible thin skin made of a PVC film. To control the camber, the MFC (Smart Material Co. / M8528P1, d33 type) actuators are embedded between the frames and skin at the distance of 8.5 cm from the flapping axis on the left and right wings.

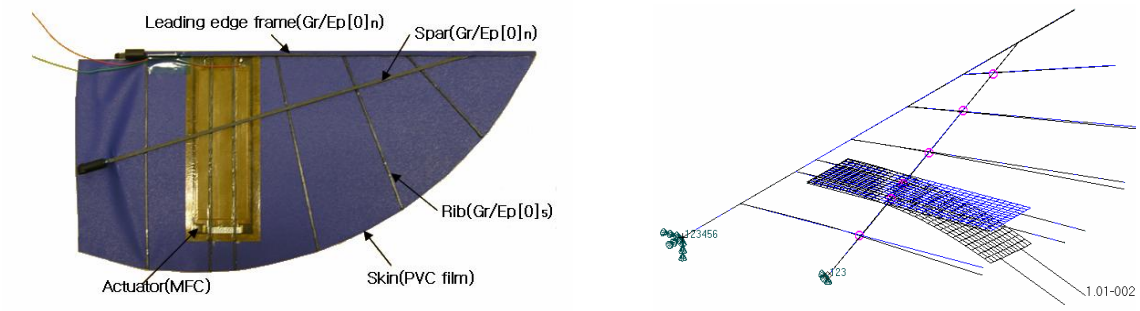

Figure 7: Configuration of smart flapping wing (left) and finite element model (right).

4.2 Performance tests

Static and dynamic tests are performed to investigate the performance of the surface actuators. The input voltage from -500V to 1500V is applied to the MFC, and the vertical displacement of the trailing edge is measured by using a laser displacement sensor (LK081/LK2101). For the dynamic test, the excitation frequency range is selected to be from 1 to 8 Hz. Figures 8 and 9 show the static and dynamic test results, respectively. The displacement at the static test varies from -6.98 mm to 12.08 mm, and this deformation is 15.2% of the cord length.

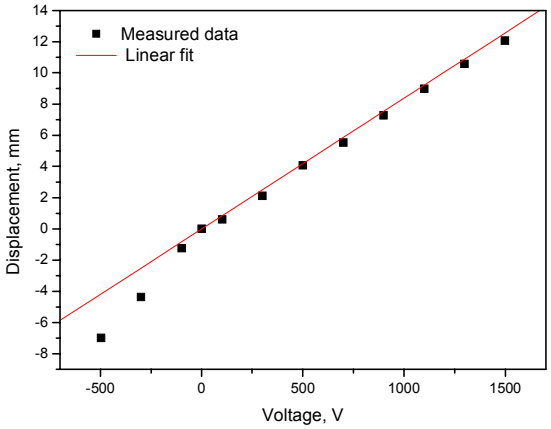

Figure 8: Static displacement of smart flapping wing.

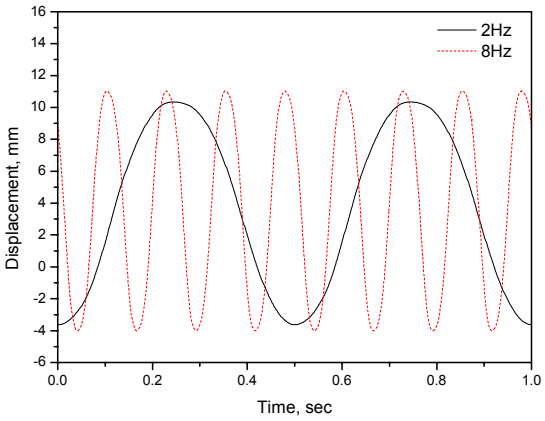

Figure 9: Dynamic displacement of smart flapping wing.

5. AERODYNAMIC TEST

5.1 Experimental setup

For the flapping test of the smart flapping wing, a flapping device is manufactured by the use of the electric motor and the transmission system of Cybird. The aerodynamic tests are performed in a subsonic wind tunnel with a test section of 1m × 0.75m × 2.2m as shown in Figure 10. Figure 11 shows the experimental test setup for the wind tunnel test. The lift (L), thrust (T) and flapping angle (S) are measured by using the test stand and the laser Doppler vibrometer (OFV-3001/303). The dynamic deformation of the wing is captured by a high speed camera (IDT XS-3). The input signals of the flapping frequency (D) and the surface actuator (U) are applied by the use of DC-power supply and Hi voltage amplifier.

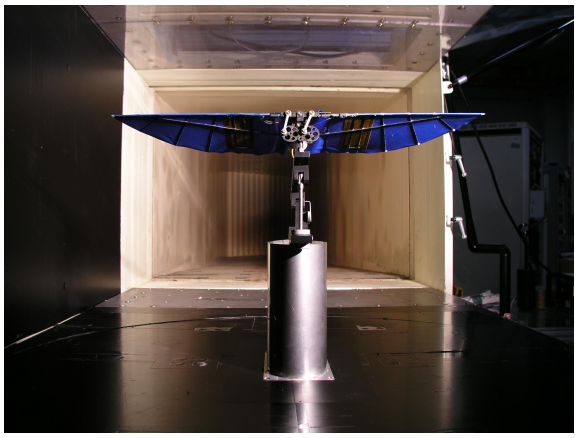

Figure 10: Wind tunnel test section and smart flapping wing.

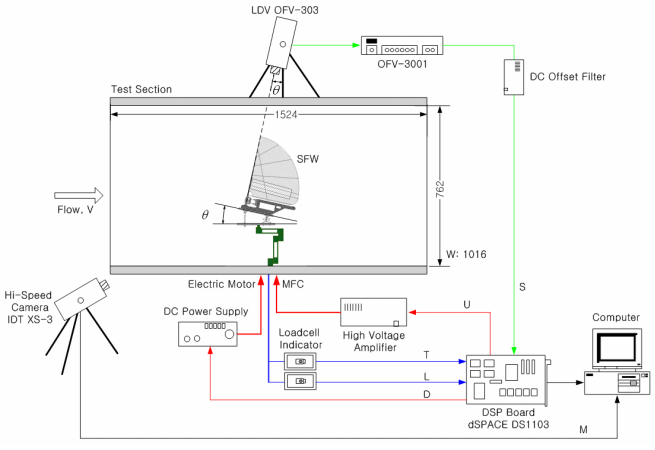

Figure 11: Experimental test setup for wind tunnel test.

A series of aerodynamic tests are performed with various values of test parameters. Table 2 shows the parameter values used in this study.

Table 2: Aerodynamic test conditions of smart flapping wing.

Velocity, V(m/s)	Angle of attack, A(deg)	Flapping frequency, F(Hz)	Actuator input voltage, U(V)
0, 2, 4, 6, 8, 10	-10, -5, 0, 5, 10, 15, 20	0 ~ 8 Hz	-500, 0, 1500

5.2 Test results

Figure 12 shows the flapping motion of the smart flapping wing measured by Hi-speed camera at V = 4m/s, F = 6Hz, U = 0V and A = 0^o. Figure 13 shows the time histories of flapping angle, lift and thrust at the same test condition. From the results, it is shown that the flapping angle varies between -25^o and 32^o, the lift has almost same frequency as the flapping angle and the thrust frequency is again two times of flapping frequency. There are distortions of the lift and thrust signals at the end of the down stroke, which may be generated by vortex which is attached to the wing. Figure 14 shows the time histories of the signals at V = 10m/s, F = 8Hz, U = -500, 0, 1500V and A = 20^o. It shows the effect of surface actuators, which is more obvious in the lift signal.

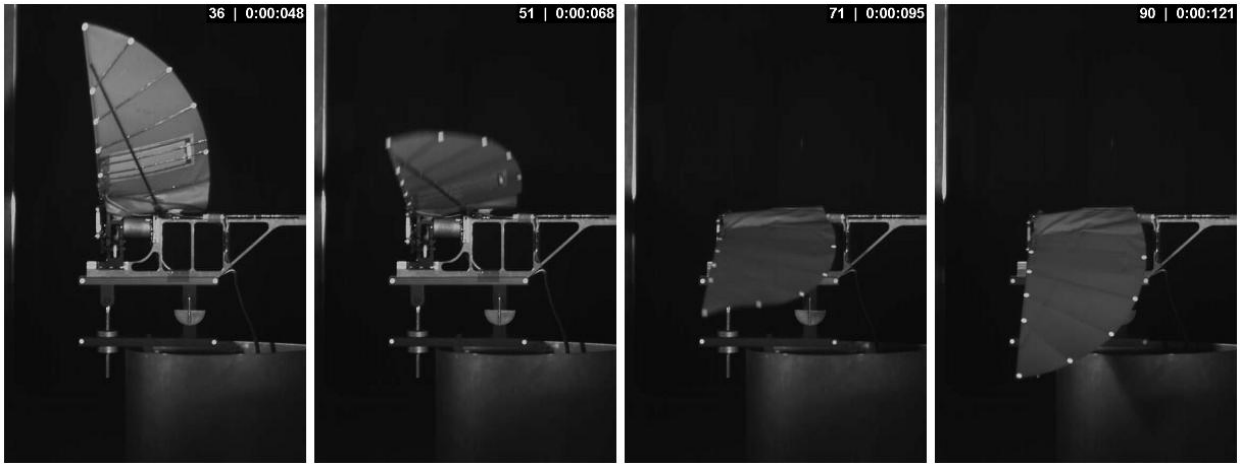

Figure 12: Flapping motion of smart flapping wing measured by Hi-speed camera.

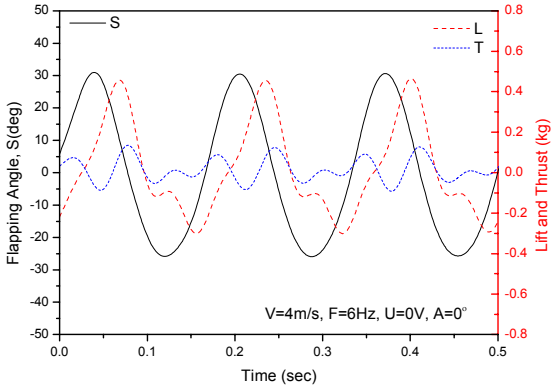

Figure 13: Comparison of lift, thrust and flapping angle at V=4m/s, F=6Hz, U=0V, A= 0^o.

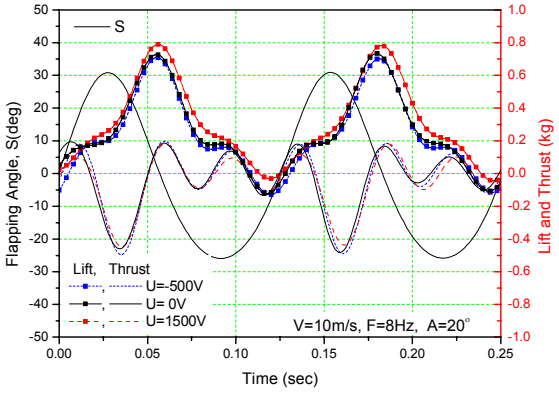

Figure 14: Comparison of lift, thrust and flapping angle at V=10m/s, F=6Hz, U=-500, 0, 1500V, A= 20^o.

5.3 Aerodynamic characteristics

From the test results, the aerodynamic characteristics of the smart flapping wing are investigated. Figure 15 shows the static lift values according to the velocity at A= -10^o , 0^o , 20^o . The lift is effectively changed by the angle of attack and the surface actuator. The maximum and minimum static lifts are 233g and -98g, respectively.

The aerodynamic lift and thrust coefficients can be expressed as follows:

$$C_L = \frac{2L}{\rho A V^2} \tag{1}$$

$$C_T = \frac{2T}{\rho A V^2} \tag{2}$$

where ρ and A are the air density and wing area, respectively. In the aerodynamic test, the air density is 1.22 Kg/m^3 and the wing area is 0.037 m^2. Figure 16 shows the lift and thrust coefficients at the static condition. From this result, it is clear that the lift coefficient has constant slope at same velocity for the surface actuator inputs. The slope decreases by increasing the velocity because of the flexibility of the wing which reduces the effective angle of attack of the wing.

Figures 17 and 18 show the mean lift and thrust coefficients according to advance ratio, *J*, which is the ratio of the flight speed to the speed of the wingtip. The advance ratio can be written as follows:

$$J = \frac{V}{2\theta f b} \tag{3}$$

where θ, f , and b are flapping amplitude, flapping frequency, and wing semi-span, respectively. From the result, it is clear that as the advance ratio is reduced below unity, the coefficients increases rapidly. It means that for the small advance ratio regime, the test condition is unsteady flight. For large advance ratio region, the variation of the coefficients is very small, which means quasi-steady flight. The results clearly show the unsteady aerodynamic characteristic.

Figure 19 shows the mean lift and thrust according to the velocity for dynamic test conditions. As the velocity increases, the surface actuator increases, and the mean lift changes up to 20% at V = 10m/s, and A = 20%. Figure 20 shows that the lift and thrust coefficients increase with increasing flapping frequency at low speed regime. It clearly demonstrates that the test condition is the unsteady flow regime, where the aerodynamic characteristics depend on dynamic stall vortex.

Figures 21 and 22 show the mean lift and the thrust maps. Form the results, it is shown that the lift is mostly effected by velocity and angle of attack, and the thrust is mostly effected by velocity and flapping frequency.

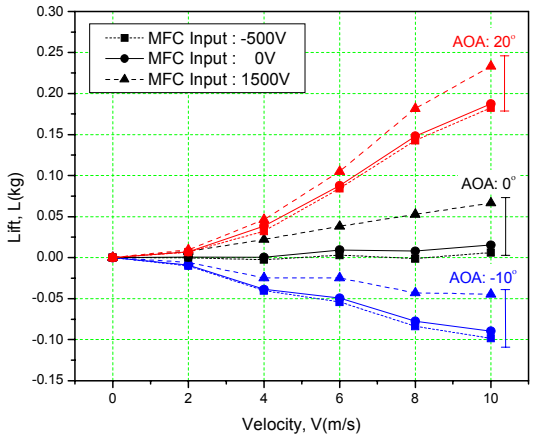

Figure 15: Angle of attack effect at static conditions, F=0Hz.

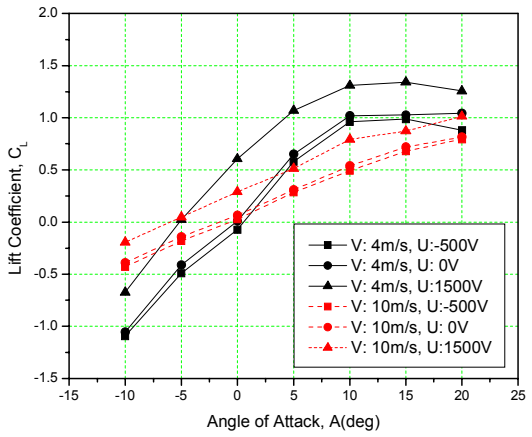

Figure 16: Comparison of lift and thrust coefficients at static conditions, F=0Hz.

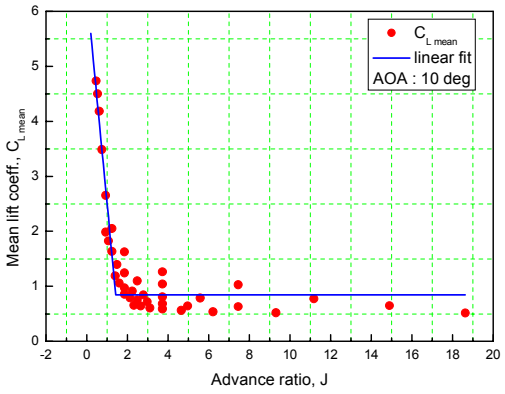

Figure 17: Unsteady aerodynamic effect of mean lift, at A= 20^{o} .

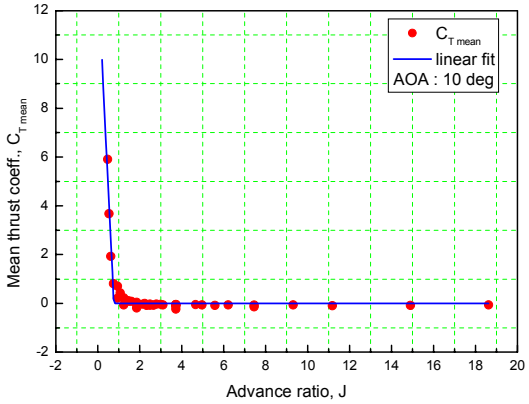

Figure 18: Unsteady aerodynamic effect of mean lift, at A= 20^{o} .

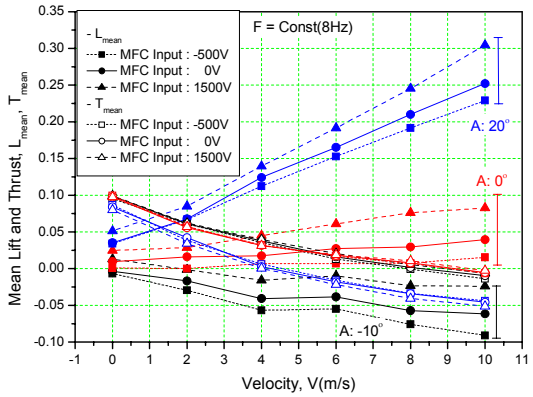

Figure 19: Surface actuator effect according to velocity.

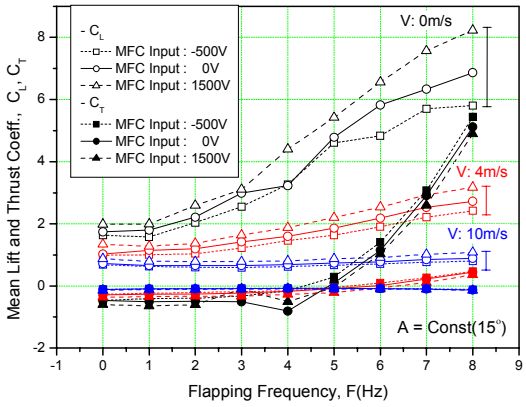

Figure 20: Surface actuator effect according to flapping frequency.

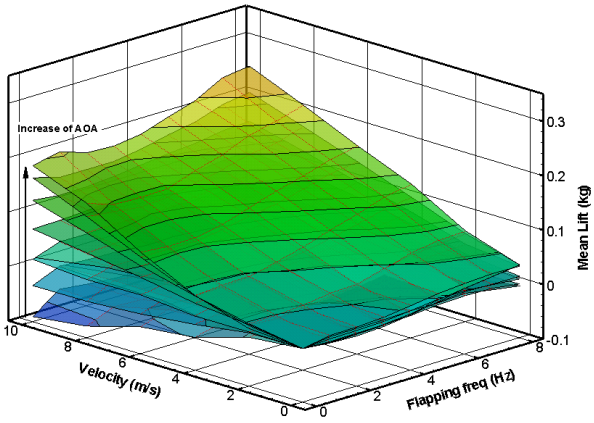

Figure 21: Mean lift maps according to velocity and flapping frequency.

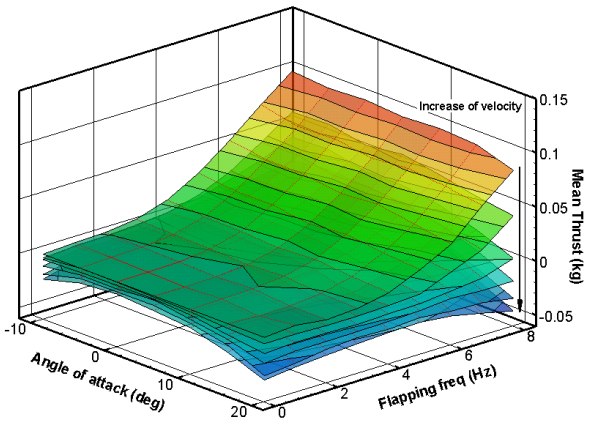

Figure 22: Mean thrust maps according to angle of attack and flapping frequency.

6. CONCLUDING REMARKS

In the present study, we developed the smart flapping wing with a MFC actuator. To mimic the bird flight, unsteady aerodynamic characteristics of bird, insect and ornithopters are investigated. For the measurement of aerodynamic forces of flapping devices, the test stand is manufactured, and dynamic test of Cybird is performed. The smart flapping wing is designed and manufactured, and static and dynamic tests are performed to investigate the performance of the surface actuators. Finally, the aerodynamic tests of the smart flapping wing in low speed wind tunnel are performed to evaluate the dynamic characteristics. Experimental results show that unsteady flow effects are increased by decreasing the advance ratio. The deformation of the wing surface generated by the MFC is enough to control the lift and thrust. The lift generated by the smart flapping wing can increase by 20% when the MFC is actuated. The test results can be useful for the development of flapping wing air vehicles.

ACKNOWLEDGEMENT

This work was supported by grant No. **R01-2005-000-10848-0** from the Basic Research Program of the Korea Science & Engineering Foundation.

REFERENCES

1. W. Shyy, M. Berg, and D. Ljungqvist, "Flapping and Flexible Wings for Biological and Micro Air Vehicles," Progress in Aerospace Sciences, Vol. **35** pp. 455-505, 1999.
2. T.N. Pornsin-sirirak, Y.C. Tai, C.M. Ho, and M. Keennon, "Microbat: A Palm-Sized Electrically Powered Ornithopter," 2001 NASA/JPL Workshop on Biomorphic Robotics, Pasadena, CA, August 14-16, 2000.
3. T.N. Pornsin-sirirak, Y.C. Tai, H. Nassef, and C.M. Ho, "Titanium-alloy MEMS Wing Technology For a Micro Aerial Vehicle Application," Sensors and Actuators A, Vol. **89**, pp. 95-103, 2001.
4. T.N. Pornsin-sirirak, M. Liger, Y.C. Tai, S. Ho, and C.M. Ho, "Flexible Parylene-Valved Skin For Adaptive Flow Control," The 15th IEEE International MEMS Conference, Las Vegas, January 20-24, 2001.
5. M. Liger, T.N. Pornsin-sirirak, Y.C. Tai, S. Ho, and C.M. Ho, "Large-Area Electrostatic-Valved Skins For Adaptive Flow Control on Ornithopter Wings," Solid-state Sensor, Actuator, and Microsystems Workshop, January 2-6, 2002
6. K.D. Jones, and M.F. Platzer, "Flapping-Wing Propulsion for a Micro Air Vehicle," the 38th Aerospace Sciences Meeting & Exhibit, AIAA-2000-0897, January 10-13, 2000.
7. K.D. Jones, T.C. Lund, and M.F. Platzer, "Experimental and Computational Investigation of Flapping-Wing Propulsion for Micro Air Vehicles," Conference on Fixed, Flapping and Rotary Wing Vehicles at Very Low Reynolds Numbers, Notre Dame, Indiana, June 5-7, 2000.
8. K.D. Jones, C.J. Bradshaw, J. Papadopoulos, and M.F. Platzer, "Improved Performance and Control of Flapping-Wing Propelled Micro Air Vehicles" the 42nd Aerospace Sciences Meeting & Exhibit, AIAA-2004-0399, January 5-8, 2004.
9. H.C. Park, K.J. Kim, S.K. Lee, and Y.J. Chah, "Electromechanical Flapping produced by Ionic Polymer-Metal Composites," SPIE's Smart Structures and Materials 2005, Vol. **5385**, San Diego, 2004.
10. M. Syaifuddin, H.C. Parkim, K.J. Yoon, and N.S. Goo, "Design and evaluation of LIPCA-actuated flapping device," SPIE's Smart Structures and Materials 2005, Vol. **5764**, San Diego, 2005.
11. S. Shigeru, Z. Lijiang, and K. Keiji, "The Relationship between Dragonfly Wing Structure and Torsional Deformation," Journal of Theoretical Biology, Vol. **193**, pp.39-45, 1998.
12. R. Dudley, "Unsteady Aerodynamics," Science, Vol. **284**, pp. 1937-1939, 1999.
13. J.D. Delaurier, "An Ornithopter Wing Design," Canadian Aeronautics and Space Journal, Vol. **40**, No. 1, pp. 11-18, March, 1994.
14. Cote F., Masson P., Mrad N., and Cotoni V., "Dynamic and static modelling of piezoelectric composite structures using a thermal analogy with MSC/NASTRAN," Composite Structures, Vol. **65**, pp. 471-484, 2004.